ELSEVIER
Nanomedicine: Nanotechnology, Biology, and Medicine
xx (xxxx) xxx–xxx
nanomedicine Nanotechnology, Biology, and Medicine
Original Article
nanomedjournal.com

Cationic carrier peptide enhances cerebrovascular targeting of nanoparticles in Alzheimer's disease brain

Kristen M. Ahlschwede, PhD[a,b,f], Geoffry L. Curran, MS[b], Jens T. Rosenberg, PhD[d], Samuel C. Grant, PhD[c,d], Gobinda Sarkar, PhD[e], Robert B. Jenkins, PhD[e], Subramanian Ramakrishnan, PhD[d,e], Joseph F. Poduslo, PhD[b], Karunya K. Kandimalla, PhD[a,b,*]

[a]*Department of Pharmaceutics and Brain Barriers Research Center, College of Pharmacy, University of Minnesota, Minneapolis, MN, USA*
[b]*Molecular Neurobiology Laboratory, Departments of Neurology, Neuroscience and Biochemistry/Molecular Biology, Mayo Clinic College of Medicine, Rochester, MN, USA*
[c]*The Florida State University and National High Magnetic Field Laboratory, Tallahassee, FL, USA*
[d]*Department of Chemical & Biomedical Engineering, FAMU-FSU College of Engineering, Florida State University, Tallahassee, FL, USA*
[e]*Department of Experimental Pathology, Mayo Clinic College of Medicine, Rochester, MN, USA*
[f]*Department of Pharmaceutical Sciences, College of Pharmacy, Rosalind Franklin University of Medicine and Science, North Chicago, IL, USA*

Received 9 May 2018; accepted 13 September 2018

Abstract

Accumulation of amyloid beta (Aβ) peptides in the cerebral vasculature, referred to as cerebral amyloid angiopathy (CAA), is widely observed in Alzheimer's disease (AD) brain and was shown to accelerate cognitive decline. There is no effective method for detecting cerebrovascular amyloid (CVA) and treat CAA. The targeted nanoparticles developed in this study effectively migrated from the blood flow to the vascular endothelium as determined by using quartz crystal microbalance with dissipation monitoring (QCM-D) technology. We also improved the stability, permeability, and blood–brain barrier (BBB) transcytosis of targeted nanoparticles by coating them with a cationic BBB penetrating peptide (K16ApoE). The K16ApoE-Targeted nanoparticles demonstrated specific targeting of vasculotropic DutchAβ40 peptide accumulated in the cerebral vasculature. Moreover, K16ApoE-Targeted nanoparticles demonstrated significantly greater uptake into brain and provided specific MRI contrast to detect brain amyloid plaques.

Key words: Targeted nanoparticles; BBB permeating peptide; Cerebrovascular amyloid; Alzheimer's disease (AD); Magnetic resonance imaging (MRI)

Alzheimer's disease (AD) is one of the top 10 leading causes of death in the United States, and AD-associated deaths have almost doubled since 2000.[1] Hence, early diagnostic and treatment strategies for the AD are the need of the hour. Alzheimer's disease (AD) brain manifests cerebrovascular amyloid (CVA) deposits, constituting of amyloid beta (Aβ) proteins, as well as parenchymal amyloid plaques and intraneuronal tangles. Approximately, 90% of AD patients and 30% of individuals over 60 years of age have CVA.[2] AD subjects with CVA show more rapid decline in cognitive test performance than those devoid of CVA.[1]

Currently, there are no diagnostic agents for detecting cerebrovascular amyloid in AD brain; in fact, the diagnosis is only confirmed post-mortem. Treatment is limited to palliative measures, and preventive measures are unavailable, which presents a poor prognosis for the millions of people at risk. Diagnostic agents, such as Florbetapir F18, can detect the presence of amyloid

Declaration of conflicting interests: The author(s) declared no potential conflicts of interest with respect to the research, authorship, and/or publication of this article.

Funding: This work was supported by Support of Minnesota Partnership for Biotechnology and Medical Genomics grant is acknowledged. A portion of this work was performed at the National High Magnetic Field Laboratory which is supported by the State of Florida and the National Science Foundation (DMR-1157490 and DMR-1644779).

*Corresponding author at: Department of Pharmaceutics, College of Pharmacy, University of Minnesota, Minneapolis, Minnesota, USA.
E-mail address: kkandima@umn.edu (K.K. Kandimalla).

https://doi.org/10.1016/j.nano.2018.09.010
1549-9634/

but are non-selective to cerebrovascular amyloid. Our previous studies have shown that the nanoparticle targeted with human anti-amyloid antibody IgG4.1, aided in the detection of cerebrovascular amyloid.[2–4] These studies have demonstrated that the recognition and high-affinity binding of IgG4.1 to cerebrovascular amyloid (CVA) facilitates the early detection of CVA in the AD brain. However, this goal is achieved effectively only when the nanoparticles are internalized by the BBB endothelium after evading peripheral clearance processes and subsequently retained in the cerebral vasculature. Previously, chitosan was shown to enhance the circulatory lifetime of poly lactic-co-glycolic acid (PLGA) nanoparticles and provide targeting to CVA deposits.[2] This positively charged polymer also improved the uptake of nanoparticles by the brain endothelial cells, but transcytosis across BBB endothelial cells remained limited.

To surmount this limitation and deliver sufficient payload for therapy, nanoparticles should be designed to exploit the transcellular transport processes in the BBB endothelial cells. Permeability at the BBB endothelium can be improved by increasing cationic charge density on the nanoparticle. It has been shown that a positively charged polyamine modified anti-amyloid antibody fragment conjugated to the nanoparticle surface can improve the BBB permeability of nanoparticles.[5] Similarly, cationic carrier peptides can also be conjugated to the surface to achieve a similar effect.[6] However, both systems typically require an additional conjugation step, which may interfere with the integrity of IgG4.1. However, K16ApoE, a cationic carrier peptide composed of 16 lysine residues and amino acids 151–170 of the low-density lipoprotein receptor (LDLR)-binding segment of the apolipoprotein E (ApoE) peptide, is a "mix-and-go" system and does not require any conjugation to the nanoparticle surface. The K16ApoE was shown to increase the brain uptake of cisplatin by 34-fold[7] and that of non-specific IgG/IgM antibodies by 5-fold.[8] In this study, we employed K16ApoE to improve the permeability of nanoparticles across the BBB.

Materials and methods

Materials

Acid terminated poly lactic-co-glycolic acid (PLGA) containing lactic acid and glycolic acids in 50:50 ratio (MW 153,000) was generously provided by Corbin (Gorinchem, Netherlands). The IgG4.1, a monoclonal antibody raised against human fibrillary Aβ42, was developed at the Mayo Clinic (Rochester, MN), whereas DutchAβ40, fluorescein-labeled DutchAβ40 (F-DutchAβ40) and K16ApoE were synthesized by the Mayo Clinic Proteomic Core Facility. Bicinchoninic acid (BCA), protein assay kit, was procured from Thermo Fisher Scientific (Waltham, MA). All cell culture reagents were obtained from Mediatech, Inc. (Manassa, VA). The human cerebral microvascular endothelial cell line (hCMEC/D3) was donated by P-O Couraud, Institut (Cochin, France). All other chemicals were purchased from Sigma-Aldrich (St. Louis, MO).

Animals

Eight-week-old wild-type (WT, B6/SJL) mice were obtained from Jackson Laboratories (Bar Harbor, ME). The APP transgenic mice (Tg2576) were purchased from Taconic (Germantown, NY) and housed under standard conditions in the non-barrier facility and provided access to food and water ad libitum. Twelve wild-type mice and four Tg2576 mice were used for these studies. All studies were conducted in accordance with National Institutes of Health Guide for the Care, and Use of Laboratory Animals and the protocols were approved by Mayo Clinic Institutional Animal Care and Use Committee.

Cell culture

Madin Darby Canine Kidney (MDCK) cells were cultured in media composed of 90% DMEM, 10% fetal bovine serum and 1% penicillin–streptomycin. Human brain microvascular endothelial cells (hCMEC/D3) were cultured as described elsewhere.[9] The hCMEC/D3 cells were seed on 12 mm Transwells® (Costar, Cambridge, MA) pre-coated with 0.1% type 1 rat-tail collagen. The Transwells® were cultured for 7 days under 5% CO_2 at 37 °C and were used for the experiments when the monolayer exhibited a transendothelial electrical resistance (TEER) value greater than 75 Ω/cm^2.

Preparation of curcumin-loaded PLGA nanocore

The PLGA nanocore was prepared using a modified emulsion technique described in our earlier publication.[2] Briefly, the organic phase consisting of 20 mg/mL PLGA and 1 mg/mL curcumin was dissolved in methylene chloride and slowly added under constant stirring at 1500 rpm to an aqueous phase consisting of 1% polyvinyl alcohol in distilled water with constant stirring at 1500 rpm.[10,11] After the formation of a stable emulsion, an equal volume of water was added, and the excess methylene chloride was evaporated in a water bath maintained at 45 °C. Large particles were removed from the PLGA nanocore suspension by centrifugation at 5000 rpm for 10 min.

Modification of PLGA-nanocore surface

Preparation of gadolinium-diethylene triamine pentaacetic acid ([Gd]DTPA) conjugated chitosan

The [*Gd]DTPA*, a magnetic resonance imaging (MRI) contrast agent, was conjugated to medium molecular weight chitosan (MW = 190,000–310,000 Da) by carbodiimide reaction.[5,12,13] The *[Gd]DTPA*-chitosan was dialyzed against 1 L of distilled water using a Spectrapor 7 dialysis membrane (MW cut-off of 50,000 Da) to remove unconjugated *[Gd]DTPA*. Then the *[Gd]DTPA*-chitosan was lyophilized and stored at 4 °C.

Conjugation of chitosan to the nanoparticle surface

A solution containing 500 μg/mL *[Gd]DTPA*-chitosan and 1.5 mg/mL of low molecular weight chitosan (MW = 50,000–190,000 Da) were covalently conjugated to 5 mL of freshly prepared curcumin-loaded PLGA nanocore via carbodiimide method. The nanoparticles thus formed were centrifuged at 12,000 rpm for 10 min to remove free chitosan and curcumin.[14]

Radioiodination of IgG4.1

IgG4.1 was labeled with $Na^{125}I$ using the chloramine-T procedure described, previously.[15,16] Free ^{125}I was removed from

the labeled IgG4.1 by dialysis in 0.01 M phosphate-buffered saline (PBS) at pH 7.4.

Conjugation of anti-amyloid antibody to the nanoparticle surface

The IgG4.1 or ^{125}I- IgG4.1 was conjugated to the nanoparticle surface by the carbodiimide reaction at pH 5, with constant stirring at 200 rpm in an ice bath. Targeted nanoparticles thus formed will be separated from the unconjugated IgG4.1 by centrifugation at 12,000 rpm for 10 min.[14] The amount of IgG4.1 retained on the targeted nanoparticle surface was quantified by a BCA protein kit.

Physical absorption of K16ApoE to targeted nanoparticle

Immediately before each experiment, 300 μg of K16ApoE was incubated with 5 mL of targeted nanoparticle suspension at room temperature for 60 min.[7,8]

Nanoparticle characterization

Particle size and zeta potential

Particle size (hydrodynamic diameter) of nanoparticles (without IgG4.1) and targeted nanoparticles (with IgG4.1) was measured using BI-200SM laser light scattering instrument, whereas the zeta potential was measured with Zeta Plus instrument (Brookhaven Instruments, Holtsville, New York). The K16ApoE-targeted nanoparticle morphology was characterized using an atomic force microscope (AFM) equipped with MultiMode Scanning Probe (Veeco Metrology Inc., Plainview, NY).[3]

Encapsulation efficiency and release of curcumin from the targeted nanoparticles

The encapsulation efficiency of curcumin was determined by measuring the fluorescence intensities of the pellet (encapsulated) and supernatant (free) after centrifugation.[3] To quantify the amount of curcumin released from the targeted nanoparticles, 25 mg of freshly prepared targeted nanoparticle were suspended in 3 mL distilled water, placed in a dialysis bag (MWCO = 50,000), immersed in 500 mL of PBS at 25 °C, and constantly stirred at 300 rpm. The external medium was sampled at predetermined time points up to 90 hr., and an equal amount of PBS was added to maintain a constant volume of the external medium. The curcumin fluorescence in the samples was measured at excitation and emission wavelengths of 488 and 535 nm, respectively.

Assessing the stability of ^{125}I-IgG4.1conjugated to the targeted nanoparticles

A 100 μCi aliquot of freshly prepared targeted nanoparticle suspension was added to 3 mL of distilled water. Then, 200 μL samples were collected at various time points, centrifuged at 12,000 rpm and the radioactivity was assayed in the pellet as well as the supernatant. The higher density of the PLGA polymer (~1.3 g/cm^3) allowed for the easy separation of free ^{125}I-IgG4.1 from the targeted nanoparticles.

Targeted nanoparticles bind to DutchAβ40

Binding of targeted nanoparticles to DutchAβ40 was determined using enzyme-linked immunosorbent assay (ELISA).[17] The DutchAβ40 (10 μg/mL) was added to wells of a high protein binding plate and incubated overnight. Then the contents were aspirated, the plate was washed, bovine serum albumin was added to the plate and incubated for 1 hr. to block non-specific binding. Nanoparticles or targeted nanoparticles with and without K16ApoE were added and incubated for 3 h at 37 °C. A secondary antibody, IgG anti-mouse alkaline phosphatase, was used to detect the amount of IgG4.1 bound to DutchAβ40.

Targeted nanoparticle characterization

Migration of targeted nanoparticles

Quartz crystal microbalance-dissipation (QCM-D) method was used to estimate the migration of targeted nanoparticles towards the biosensor. To construct the biosensor, quartz crystals equipped with gold electrodes were seeded with 5000 MDCK cells.[3] After reaching confluence, which usually took 5 days, the biosensors were placed in the QCM-D chamber, and 0.1% bovine serum albumin (BSA) in Hank's balanced salt solution (HBSS) was introduced at a flow rate of 0.1 mL/min for 5 min at 37 °C. Excess BSA was removed from the biosensor by passing HBSS-HEPES at the rate of 0.1 mL/min for 3 min. The biosensors were then primed with either 500 μl HBSS (control) or 12.5 μg of DutchAβ40 in 500 μL HBSS (treatment) and then washed by passing 400 μl of HBSS-HEPES at 100 μL/min. Targeted nanoparticles (15 mg/mL) were immediately introduced at a continuous rate of 0.1 mL/min. The mass adsorbed per unit area (m) of the crystal surface was calculated using the following equation:

$$\Delta m = -\frac{\Delta F \text{ x } C}{n} \quad (1)$$

where ΔF is the change in frequency, C = mass sensitivity constant (17.7 ng·cm^{-2}·Hz^{-1}) and n = overtone number, which was 5.

Uptake of targeted nanoparticles by hCMEC/D3 cells

An in vitro BBB model was prepared by seeding hCMEC/D3 cells on collagen-coated Transwells® (12 mm, Costar, Cambridge, MA). The polarized monolayer of hCMEC/D3 cells thus formed was pretreated with 25 μg/mL of DutchAβ40 protein for 30 min.[3,4] Then 30 mg/mL of targeted nanoparticles, conjugated with AlexaFluor 647 labeled IgG4.1, were added and incubated at 37 °C under 5% CO_2 for 60 min. Then the Transwells® were thoroughly washed and fixed with 4% paraformaldehyde, stained with Hoechst, mounted, and imaged with Zeiss LSM 510 (Carl Zeiss Inc., Thornwood, New York). The filters used for imaging were: 350/470 nm-Hoechst; 488/520 nm-fluorescein; and 652/668- Alexa Fluor647.

In vivo characterization

Biodistribution of ^{125}I-targeted nanoparticles

The brain and peripheral organ distribution of ^{125}I-targeted nanoparticles and K16ApoE- ^{125}I-targeted nanoparticles was evaluated in WT mice anesthetized with 1.5% isoflurane in 4 L/min O_2. An IV bolus dose of DutchAβ40 protein (1 mg in 100 μL; treatment) or normal saline (100 μL; control) was administered via the femoral vein as described previously.[3,4] At 15 min after the injection, an IV bolus dose of ^{125}I-targeted nanoparticles (100 μCi in 100 μL) was administered by the femoral vein. Blood samples (20 μL) were collected from the femoral artery at various time points up to 60 min. Plasma was recovered from the blood samples and assayed for radioactivity using a two-channel gamma counter (Cobra II; Amersham Biosciences Inc., Piscataway, NJ). Plasma area under the curve

Table 1
The average particle size and zeta potential of nanoparticles (without IgG4.1), targeted-nanoparticles (with IgG4.1), and targeted-nanoparticles with K16ApoE at pH 7.0.

Formulation	Particle size (nm)	Zeta Potential (mV)
Nanoparticles (without IgG4.1)	220 ± 9	7.45 ± 0.32
Targeted nanoparticles	223 ± 16	1.99 ± 0.08
K16ApoE-Targeted Nanoparticles	235 ± 10	4.88 ± 0.08

Data presented as mean ± standard error of the mean (SEM). The particle size measurements of various nanoparticles are not significantly different (n = 3). $P < 0.001$ (n = 3): zeta potential values of targeted nanoparticles versus K16ApoE-targeted nanoparticles.

(AUC) of radioactivity was determined using the trapezoidal rule. At 60 min, the mice were transcardially perfused with PBS; brain and peripheral clearance organs, such as liver and kidneys, were removed and weighed; and immediately assayed for radioactivity.

Molecular imaging

A 200 μL aliquot of targeted nanoparticles or K16ApoE-targeted nanoparticles (75 μg/μL) was injected into the femoral vein of two-year-old APP transgenic (Tg2576) mice. After 3 h, the mice were subjected to transcardial perfusion with PBS followed by 4% paraformaldehyde. Brains were removed, immediately immersed in 4% paraformaldehyde and stored at 4 °C. Before MR imaging, the brain samples were washed in PBS for 24 hr. and placed in a 10-mm NMR tube (Wilmad GlasLab, Buena, NJ) containing fluorinert (3 M, St. Paul MN), a perfluorinated liquid that has no ^{1}H MRI background signal.[18,19] All brains were imaged with 21.1 T (900 MHz) magnet at the National High Magnetic Field Laboratory (NHMFL, Tallahassee, FL).[20,21] This magnet is equipped with a Bruker Avance III console and Paravision 5.1 (Bruker Biospin, Billerica, MA). Both the samples were imaged in unison using a 33-mm birdcage coil together with a 63-mm (inner diameter) gradient capable of producing a peak gradient strength of 600 mT/m (Resonance Research Inc. Billerca MA). High-resolution T_2^* weighted images were obtained by a 3D gradient recalled echo sequence (GRE). The matrix was set to achieve a 50-μm isotropic resolution. The echo (TE) and repetition (TR) times were 5 and 150 ms, respectively, and the scan time was 10 hr. The data set was processed with AMIRA 5.3.3 (Visage Imaging, CA) software using a Gaussian filter. This software was also used to present the 3D data set and to show the regions of interest.

Statistical analysis

One-way analysis of variance (ANOVA) followed by Tukey's post-tests were employed.

Results

Physical characterization of nanoparticles (without IgG4.1) and targeted nanoparticles (with IgG4.1)

Particle size and zeta potential measurements

The average particle size was 220 ± 8.9 nm and 223 ± 16 nm for nanoparticles with and without IgG4.1, respectively (Table 1).

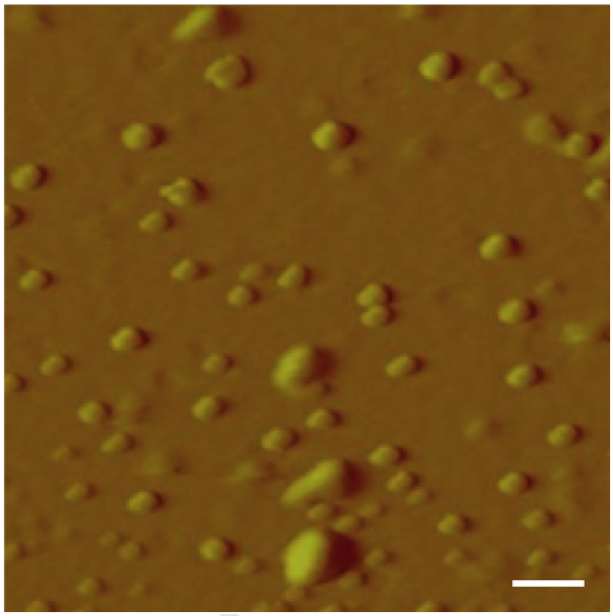

Figure 1. The atomic force micrograph of K16ApoE-targeted nanoparticles. Scale bar, 200 nm.

Upon conjugation of IgG4.1, the zeta potential decreased from 7.45 ± 0.32 mV to 1.99 ± 0.08 mV (Table 1). Following physical adsorption of K16ApoE to the surface, the hydrodynamic radius slightly increased to 235 ± 10 nm, and the corresponding zeta potential also increased to 4.88 ± 0.08 mV compared to targeted nanoparticles without the K16ApoE peptide. The particle sizes in various nanoparticle formulations are not significantly different. The AFM micrograph of the K16ApoE-targeted nanoparticles showed that the majority of nanoparticles are spherical with ~100 nm in size (Figure 1).

Encapsulation efficiency and release of curcumin

Targeted nanoparticles contained 409 ± 1.7 ng/mg of curcumin, and represented an encapsulation efficiency of 72%. Curcumin exhibited a slow release from the targeted nanoparticles with less than 10% of curcumin released in 90 hr. (Figure 2, *A*). The release profile appeared sigmoidal without the characteristic burst effect.

Quantification of IgG4.1 on the targeted nanoparticle surface

The amount of IgG4.1 conjugated to targeted nanoparticles was 11.7 ± 0.7 μg/mg, as determined by BCA assay (data not shown). The low amount of ^{125}I-IgG4.1 released (5% over the course of 48 h) from the nanoparticle surface (Figure 2, *B*) indicates that ^{125}I-IgG4.1 was stably conjugated to the targeted nanoparticles.

Binding of various nanoparticles to DutchAβ40

As expected, blank nanoparticles without IgG4.1 (control) did not bind significantly to DutchAβ40, whereas targeted nanoparticles, with and without K16ApoE, showed 5–6 fold increase in binding to DutchAβ40 compared to the blank nanoparticles (Figure 3).

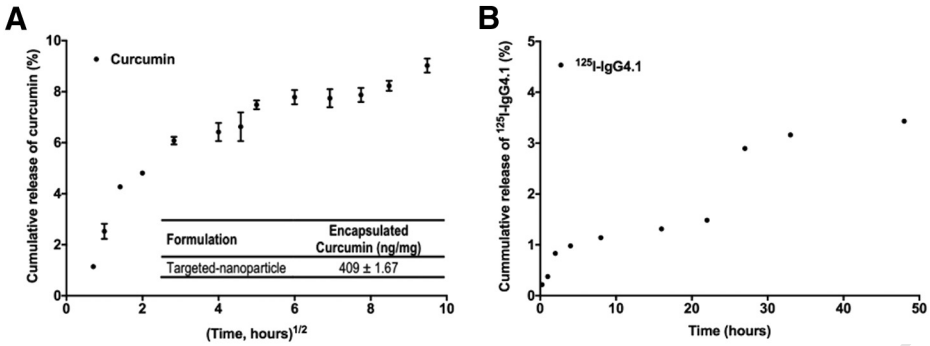

Figure 2. **(A)** The cumulative release of curcumin from the targeted nanoparticles. (Table insert) The amount of encapsulated curcumin in the targeted-nanoparticles formulation. **(B)** The cumulative release of ^{125}I-IgG4.1 from targeted nanoparticles.

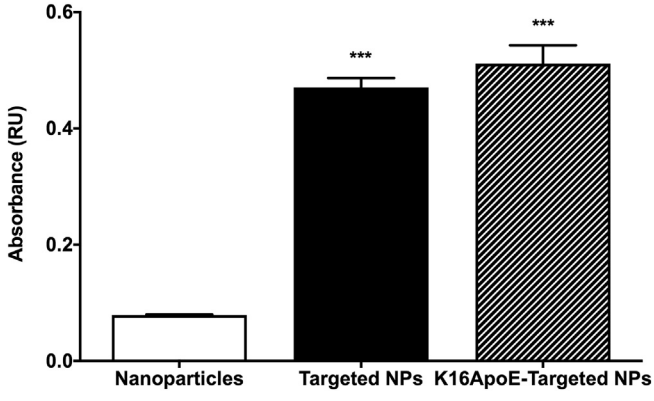

Figure 3. **(A)** The ability of the nanoparticles (Nanoparticles- without IgG4.1), targeted nanoparticles (Targeted NPs- with IgG4.1) and K16ApoE-targeted NPs to recognize and bind to fibrillary DutchAβ40. Data presented as a mean ± standard error of the mean (SEM) (n = 3). One-way ANOVA followed by Tukey's multiple comparison tests have shown ***$P < 0.001$: Nanoparticles versus Targeted NPs; Nanoparticles versus K16ApoE-Targeted NPs.

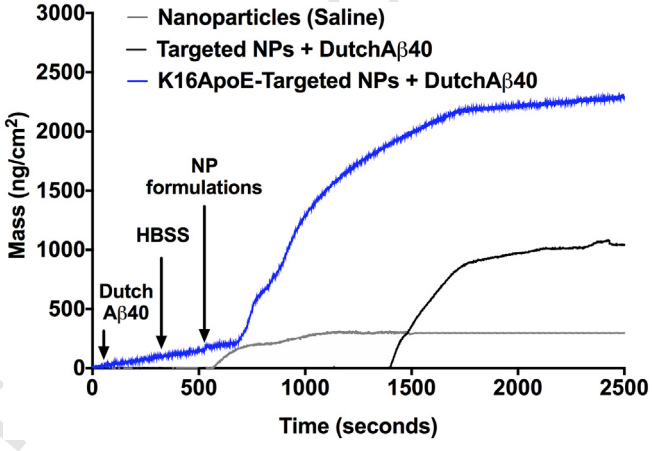

Figure 4. The ability of Nanoparticles, targeted nanoparticles (Targeted NPs), and targeted nanoparticles with K16ApoE (K16ApoE-Targeted NPs) to migrate towards DutchAβ40-treated (treatment) or HBSS treated (control) biosensors.

Migration of targeted nanoparticles towards DutchAβ40 treated biosensors

The blank nanoparticles showed minimal adsorption to HBSS treated biosensors (gray), which was constructed by growing a monolayer of MDCK cells on a quartz crystal sensor (Figure 4). A 6-fold increase in mass per unit area was observed due to the adsorption of K16ApoE-targeted nanoparticles as compared to targeted nanoparticle without K16ApoE on HBSS treated biosensor (Figure 4). Initially, the nanoparticle uptake was linear; but, the uptake saturated over longer exposure times.[3] Treatment of a biosensor with DutchAβ40 triggered a 3 to 4-fold increase in the uptake of targeted-nanoparticles without K16ApoE. However, K16ApoE-targeted nanoparticles demonstrated the highest adsorption to DutchAβ40 treated biosensors and exhibited a further two-fold increase over that of targeted nanoparticles without K16ApoE (Figure 4).

The uptake of targeted nanoparticles in the in vitro BBB model

The uptake of AF647 tagged targeted nanoparticles by the hCMEC/D3 monolayers pretreated with F-DutchAβ40 was examined using laser confocal microscopy. The z-stack image showed intra-endothelial accumulation of AF647 tagged targeted nanoparticles as well as F-DutchAβ40 (Figure 5). The uptake of AF647-K16ApoE-targeted nanoparticles was substantially greater than the AF647-targeted nanoparticles. Moreover, the co-localization of AF647-K16ApoE-targeted nanoparticles (red fluorescence) with DutchAβ40 (green fluorescence) was also substantially higher (Figure 5).

In vivo distribution of the targeted nanoparticles

The K16ApoE-targeted nanoparticles showed 8 to 10-fold higher accumulation in various brain regions of DutchAβ40 treated WT mice as compared to the targeted nanoparticles without K16ApoE (Figure 6, *A*). Moreover, the plasma counts of ^{125}I-targeted nanoparticles in DutchAβ40 treated mice were higher than that of K16ApoE-^{125}I-targeted nanoparticles (Figure 6, *B*). The plasma area under the curve (AUC) of ^{125}I-targeted nanoparticles was 3.7 times higher in saline-treated mice compared to that in DutchAβ40 treated mice (Table 2), whereas the plasma AUC of ^{125}I-targeted nanoparticles was ~23 times higher in DutchAβ40 treated mice as compared to K16ApoE-^{125}I-targeted nanoparticles (Table 2).

The peripheral clearance organs such as liver and kidney were also assayed for radioactivity. While the ^{125}I-targeted nanoparticle accumulation in liver was not significantly different among saline

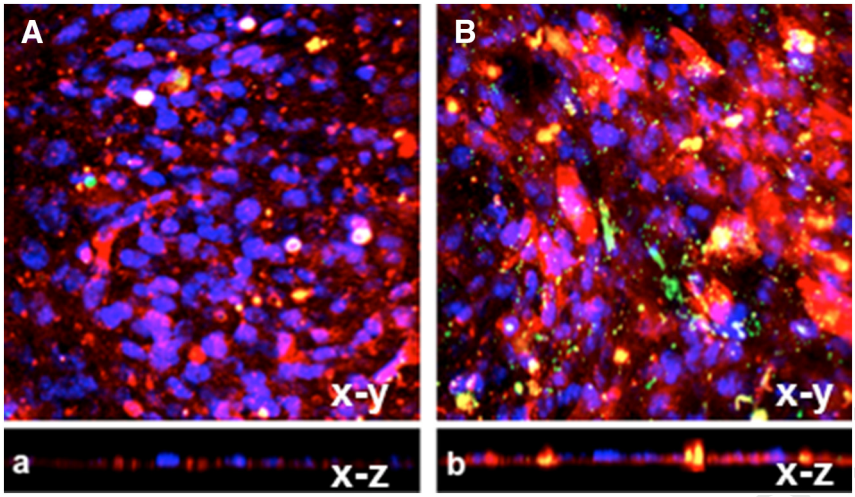

Figure 5. **(A & a)** Localization of AF647-targeted nanoparticles and **(B & b)** AF647-targeted nanoparticles with K16ApoE in polarized hCMEC/D3 monolayer. The X-Y image drawn from the middle of the Z-stack demonstrated the internalization of AF647-targeted nanoparticles with K16ApoE by endothelial cells. Projections in both the X-Z and Y-Z orthogonal planes confirm the transcytosis of AF647-targeted nanoparticles across the hCMEC/D3 monolayer. The AF647-targeted nanoparticles are shown in red fluorescence, F-DutchAβ40 with green fluorescence and blue fluorescence for the cell nucleus.

or DutchAβ40 treated mice (Figure 6, *C*); the accumulation in kidney was 2-fold higher in saline-treated mice than in DutchAβ40 treated mice (Figure 6, *C*). However, K16ApoE demonstrated no significant effect on the accumulation of ^{125}I-targeted nanoparticles in either liver or kidney.

The ability of the targeted nanoparticles formulations to detect amyloid deposits in transgenic mice

High-resolution MRI of Tg2576 transgenic mouse brains injected with targeted nanoparticles or K16ApoE-targeted nanoparticles, both containing *[Gd]DTPA,* demonstrated hypointense contrast in the hippocampus (Figure 7, *A-B*) rather than the characteristic hyperintense (bright) signal produced by *[Gd]DTPA.* This is most likely due to the localization of the nanoparticle in intracellular, vesicular or another confined volume where water exchange is insufficient, and T_2 (spin–spin relaxation) becomes the dominant contrast mechanism.[3,4,22,23]

Discussion

For targeting the cerebrovascular amyloid deposits, nanoparticles must be sufficiently small to cross the BBB, but large enough to be retained in the cerebral vasculature and not migrate into the brain parenchyma. The size of the majority of targeted nanoparticles appear to be closer to 100 nm from the AFM image (Figure 1), but their hydrodynamic diameter was 200–250 nm (Table 1). Such increase in hydrodynamic radius is not uncommon with the nanoparticles that harbor hydrophilic polymeric chains on the surface. These particles are expected to be retained in the vascular basement membrane with an estimated pore size of 100–150 nm. The physical adsorption of K16ApE to the targeted nanoparticle surface showed a modest 15 nm increase in the hydrodynamic diameter (Table 1). This increase was not statistically significant and indicates that the nanoparticles remain stable and don't aggregate in the presence of K16ApoE.

Based on our previous studies, the target zeta potential for optimal endocytosis at the negatively charged endothelial surface was 5–10 mV.[2–4] An excessively higher zeta potential increases the risk of opsonization and subsequent recognition by the reticuloendothelial system that rapidly clears nanoparticles from systemic circulation.[24] Although IgG4.1 conjugation to the surface decreased the zeta potential below the target value (Table 1), K16ApoE adsorption increased the zeta potential and moved it to the target range.

PLGA nanoparticles can efficiently entrap hydrophobic therapeutic agents such as curcumin,[14,25,26] which was previously shown to have anti-inflammatory and anti-amyloidogenic effects.[27–30] The amount of curcumin encapsulated in the targeted nanoparticles was approximately 409 ± 1.6 ng/mg of nanoparticles (Figure 2, *A*), which resulted from a reasonably high entrapment efficiency of 72%. The release of curcumin from the nanoparticles was prolonged with ~10% of the entrapped curcumin releasing within 4 days. However, the duration and extent of drug release from PLGA nanoparticles could be readily modulated by altering the relative proportions of lactic and glycolic acids used in the PLGA nanoparticle formulation.[14,25,26]

The IgG4.1 is most likely conjugated to the amine groups on chitosan, probably due to the low availability of carboxylic groups on the PLGA nanocore,[31] most likely due to their conjugation to amine groups on chitosan. The targeted nanoparticle with or without K16ApoE exhibited 6–7-fold higher binding to DutchAβ40 compared to the control nanoparticles (Figure 3). This data indicates that K16ApoE does not significantly affect the binding of the targeted nanoparticle to amyloid proteins.

The ability of the nanoparticle formulations to migrate towards the BBB endothelium was evaluated in vitro. This was accomplished by tracking the mass of nanoparticles bound to the biosensor. The migration of nanoparticles occurs by convection/diffusion processes and are affected by the size and electrostatic interactions. The targeted nanoparticles showed a minimal ability to adsorb to the blank biosensor that was not treated with DutchAβ40 (Figure 4).

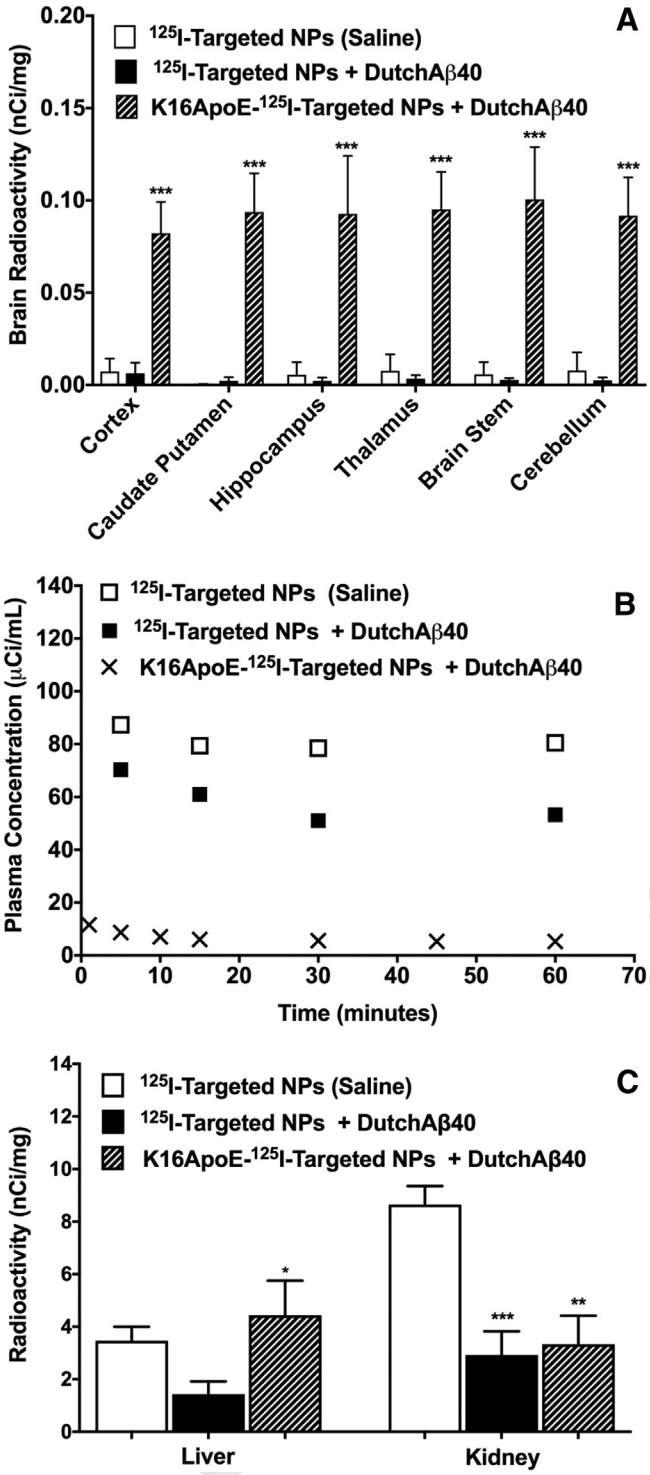

Figure 6. **(A)** The distribution of ^{125}I-targeted nanoparticles, with or without K16ApoE, in various regions of the brain of wild-type (WT) mice treated with (+) or without (–) DutchAβ40. *** $P < 0.001$ (n = 4): ^{125}I-targeted-nanoparticles with K16ApoE in DutchAβ40-treated mice vs ^{125}I-targeted-nanoparticles in DutchAβ40 or saline-treated mice in the various brain regions. **(B)** The plasma kinetics of ^{125}I-targeted-nanoparticles, with or without K16ApoE, in DutchAβ40 treated (treatment) or saline-treated (control) wild-type mice. **(C)** The distribution of ^{125}I-targeted nanoparticles, with and without K16ApoE, in the liver and kidney of DutchAβ40 or saline-treated wild-type mice. ** $P < 0.01$ (n = 4): ^{125}I-targeted-nanoparticles in saline versus DutchAβ40 treated mice; *** $P < 0.001$: ^{125}I-targeted-nanoparticles versus K16ApoE-^{125}I-targeted-nanoparticles in DutchAβ40 treated mice.

Alternatively, when the targeted nanoparticle formulation was exposed to the biosensor that was pretreated with DutchAβ40, a 3- to 4-fold increase in the binding was observed. As the sizes of various nanoparticles were similar and the differences in zeta potential were modest, the migration of nanoparticles towards the biosensor is expected to be similar. Therefore, the observed differences in the adsorption of various nanoparticles to the biosensor are most likely due to differences in their binding affinities to the biosensor.

The uptake of AF647 tagged K16ApoE-targeted nanoparticles by F-DutchAβ40 treated hCMEC/D3 endothelial cell monolayers was substantially higher as compared to the monolayers treated with the same nanoparticles that lacked K16ApoE (Figure 5). Moreover, the K16ApoE-targeted nanoparticles (red fluorescence) co-localized with F-DutchAβ40 (green fluorescence), appreciably. These results show that K16ApoE plays a major role in the uptake of the targeted nanoparticles, whereas IgG4.1 could facilitate DutchAβ40 targeting.

The plasma pharmacokinetics and brain uptake of various nanoparticles were elucidated in WT mice pre-treated with 500 μg of DutchAβ40. This method provides an extensive and consistent accumulation of DutchAβ40 in the cerebral vasculature. In DutchAβ40 treated mice, the plasma AUC of targeted nanoparticles decreased substantially (Table 2), which could be due to extensive tissue distribution facilitated by the vasculotropic DutchAβ40. Further, K16ApoE-targeted nanoparticles showed substantially lower C_0 (plasma concentration at 0 min) and plasma AUC than targeted nanoparticles without K16ApoE (Table 2). Since the plasma elimination rate constant of targeted nanoparticles is not significantly affected by K16ApoE, the lower plasma AUC could again be attributed to extensive tissue distribution promoted by the K16ApoE peptide.

The DutchAβ40 pre-injected mice showed modestly higher levels of targeted nanoparticles in the brain relative to those without the pretreatment, which suggests weakly amyloid responsive uptake of targeted nanoparticles in the brain. On the other hand, brain accumulation of K16ApoE-targeted nanoparticles was 8 to 10 times higher compared to the targeted nanoparticles without K16ApoE (Figure 6, *A*). The effect was significant in all brain tissues and demonstrated the effect of K16ApoE on the brain uptake of K16ApoE-targeted nanoparticles. In comparison, liposomes modified with the cell-penetrating peptide such as TAT and a novel protein (T7) capable of recognizing the transferrin receptor, showed a marginal ~1.6-fold increase in brain uptake as compared to liposomes without T7 and TAT.[6]

The MRI results confirm the presence of targeted nanoparticles in the brain (Figure 7, *A-B*). The dark regions indicated by the yellow circles reveal the modulation of the proton relaxation rates due to the presence of the magnetic contrast agent. These regions appear to be preferentially staining the parenchymal plaques, which is highly significant. The dominating T_2^* contrast for this agent appears hypointense (dark), which likely occurs when the agent is accumulated in intracellular vesicles or other confined spaces. These voids are likely not due to the blood residue or clotting, because the contrast is mostly seen in the brain regions where amyloid deposits are expected to be present.

Moreover, the minimal contrast in mice injected with targeted nanoparticles (without K16ApoE) provides confidence that the observed contrast is most likely due to the *[Gd]DTPA*-labeled,

Table 2
The plasma pharmacokinetic parameters of ^{125}I-targeted nanoparticles in wild type (WT) mice.

	^{125}I-targeted NPs	With DutchAβ40		P
		^{125}I-targeted NPs	K16ApoE- ^{125}I-targeted NPs	
AUC (min x μCi/ml)	26,887 ± 2100	7196 ± 2696	314.4 ± 105.9	***
K_{el} (min^{-1})	0.0025 ± 0.0007	0.0026 ± 0.0006	0.013 ± 0.006	N.S.
V_{ss} (ml/μCi)	0.94 ± 0.09	1.58 ± 0.15	15.31 ± 5.16	*

Data presented as mean ± standard error of the mean (SEM). One-way ANOVA followed by Tukey's multiple comparison test have showed: *** $P < 0.001$ (n = 4), the area under the curve (AUC) of ^{125}I-targeted nanoparticles in saline vs AUC of ^{125}I-targeted nanoparticles in DutchAβ40 treated mice; *** $P < 0.001$ (n = 4), the AUC of ^{125}I-targeted nanoparticles versus AUC of K16ApoE-^{125}I-targeted nanoparticles in DutchAβ40 treated mice; * $P < 0.05$ (n = 4): the volume of distribution at steady state (Vss) of targeted nanoparticles versus K16ApoE-targeted nanoparticles in DutchAβ40 treated mice.

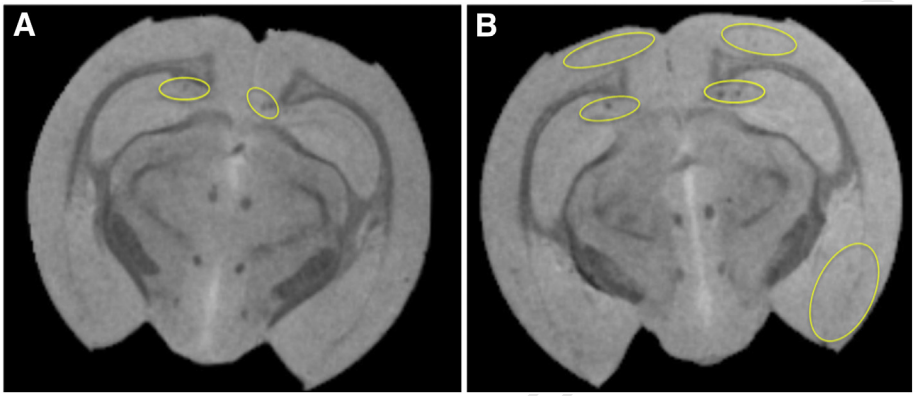

Figure 7. Magnetic resonance imaging of **(A)** *[Gd]DTPA*-targeted nanoparticles and **(B)** *[Gd]DTPA*-K16ApoE-targeted nanoparticles in APP transgenic mice. Regions marked with yellow oval shapes indicate enhanced contrast provided by nanoparticles.

K16ApoE-targeted nanoparticles.[3,4,32] The advantage the K16ApoE-targeted nanoparticles have over current FDA approved diagnostic options, such as Florbetapir F18, is their potential to detect individual plaques. However, this study does not present evidence of selective cerebrovascular amyloid targeting of nanoparticles. Curcumin-conjugated magnetic nanoparticles and IgG4.1 coated iron oxide nanoparticles were previously claimed to detect amyloid plaques in AD transgenic mice using MR imaging.[32,33] However, these nanoparticles are composed of a superparamagnetic iron oxide, which may be counter indicative as iron previously has been shown to accumulate during the progression of Alzheimer's disease.[34] Moreover, high payloads of therapeutic agents cannot be included in these nanoparticles.

In conclusion, surface conjugation of PLGA nanoparticles with chitosan and physical absorption of K16ApoE resulted in significantly greater brain uptake. This is most likely facilitated by the greater BBB permeability of K16ApoE-targeted nanoparticles and their high-affinity binding to amyloid deposits. Imaging agents and hydrophobic therapeutic agents can be readily added to this nanoparticle to facilitate the early diagnosis through MR imaging and treatment of pathological changes resulting from cerebral amyloidosis.

Acknowledgements

The authors would like to thank Professor Timothy Wiedmann for his assistance in editing the manuscript. The authors would also like to thank James Ahlschwede for his assistance in designing the graphical abstract.

References

1. Alzheimer's Association. 2017 Alzheimer's disease facts and figures. *Alzheimer's Dement* 2017;**13**(4):325-373 [Internet, Available from: http://linkinghub.elsevier.com/retrieve/pii/S1552526017300511].
2. Jaruszewski KM, Ramakrishnan S, Poduslo JF, Kandimalla KK. Chitosan enhances the stability and targeting of immuno-nanovehicles to cerebro-vascular deposits of Alzheimer's disease amyloid protein. *Nanomedicine* 2012;**8**(2):250-260.
3. Jaruszewski KM, Curran GL, Swaminathan SK, Rosenberg JT, Grant SC, Ramakrishnan S, et al. Multimodal Nanoprobes to target cerebrovascular amyloid in Alzheimer's disease brain. *Biomaterials* 2014;**35**(6):1967-1976.
4. Agyare EK, Jaruszewski KM, Curran GL, Rosenberg JT, Grant SC, Lowe VJ, et al. Engineering theranostic nanovehicles capable of targeting cerebrovascular amyloid deposits. *J Control Release* 2014;**185**(1):121-129.
5. Agyare EK, Curran GL, Ramakrishnan M, Yu CC, Poduslo JF, Kandimalla KK. Development of a smart nano-vehicle to target cerebrovascular amyloid deposits and brain parenchymal plaques observed in Alzheimer's disease and cerebral amyloid angiopathy. *Pharm Res* 2008;**25**(11):2674-2684.
6. Zong T, Mei L, Gao H, Shi K, Chen J, Wang Y, et al. Enhanced glioma targeting and penetration by dual-targeting liposome co-modified with T7 and TAT. *J Pharm Sci* 2014;**103**(12):3891-3901.
7. Sarkar G, Curran GL, Sarkaria JN, Lowe VJ, Jenkins RB. Peptide carrier-mediated non-covalent delivery of unmodified cisplatin, methotrexate and other agents via intravenous route to the brain. *PLoS One* 2014;**9**(5). Q4
8. Sarkar G, Curran GL, Mahlum E, Decklever T, Wengenack TM, Blahnik A, et al. A carrier for non-covalent delivery of functional Q5

beta-galactosidase and antibodies against amyloid plaques and IgM to the brain. *PLoS One* 2011;**6**(12).

9. Weksler B, Romero IA, Couraud P-O. The hCMEC/D3 cell line as a model of the human blood brain barrier. *Fluids Barriers CNS* 2013;**10**(1):16 [Internet, Available from: http://fluidsbarrierscns.biomedcentral.com/articles/10.1186/2045-8118-10-16].
10. Yang R, Shim WS, De Cui F, Cheng G, Han X, Jin QR, et al. Enhanced electrostatic interaction between chitosan-modified PLGA nanoparticle and tumor. *Pharm* 2009;**371**(1–2):142-147.
11. Yang R, Yang SG, Shim WS, Cui F, Cheng G, Kim IW, et al. Lung-specific delivery of paclitaxel by chitosan-modified PLGA nanoparticles via transient formation of microaggregates. *J Pharm Sci* 2009;**98**(3):970-984.
12. Saha TK, Ichikawa H, Fukumori Y. Gadolinium diethylenetriamino-pentaacetic acid-loaded chitosan microspheres for gadolinium neutron-capture therapy. *Carbohydr Res* 2006;**341**(17):2835-2841.
13. Shikata F, Tokumitsu H, Ichikawa H, Fukumori Y. In vitro cellular accumulation of gadolinium incorporated into chitosan nanoparticles designed for neutron-capture therapy of cancer. *Pharm Biopharm* 2002;**53**(1):57-63.
14. Shahani K, Swaminathan SK, Freeman D, Blum A, Ma L, Panyam J. Injectable sustained release microparticles of curcumin: a new concept for cancer chemoprevention. *Cancer Res* 2010;**70**(11):4443-4452.
15. Poduslo JF, Curran GL, Wengenack TM, Malester B, Duff K. Permeability of proteins at the blood-brain barrier in the normal adult mouse and double transgenic mouse model of Alzheimer's disease. *Neurobiol Dis* 2001;**8**(4):555-567.
16. Poduslo JF, Curran GL. Increased permeability of superoxide dismutase at the blood-nerve and blood-brain barriers with retained enzymatic activity after covalent modification with the naturally occurring polyamine, putrescine. *J Neurochem* 1996;**67**(2):734-741 [Internet, Available from: http://www.ncbi.nlm.nih.gov/pubmed/8764602].
17. Poduslo JF, Ramakrishnan M, Holasek SS, Ramirez-Alvarado M, Kandimalla KK, Gilles EJ, et al. In vivo targeting of antibody fragments to the nervous system for Alzheimer's disease immunotherapy and molecular imaging of amyloid plaques. *J Neurochem* 2007;**102**(2):420-433 [Internet, cited 2016 Nov 23, Available from: http://www.ncbi.nlm.nih.gov/pubmed/17596213].
18. Ma Y, Hof PR, Grant SC, Blackband SJ, Bennett R, Slatest L, et al. A three-dimensional digital atlas database of the adult C57BL/6J mouse brain by magnetic resonance microscopy. *Neuroscience* 2005;**135**(4):1203-1215.
19. Webb AG, Grant SC. Signal-to-noise and magnetic susceptibility trade-offs in solenoidal microcoils for NMR. *J Magn Reson B* 1996;**113**(1):83-87.
20. Fu R, Brey WW, Shetty K, Gor'kov P, Saha S, Long JR, et al. Ultra-wide bore 900 MHz high-resolution NMR at the National High Magnetic Field Laboratory. *J Magn Reson* 2005;**177**(1):1-8.
21. Markiewicz WD, Brey WW, Cross TA, Dixon IR, Gor'kov PL, Grant SC, et al. A decade of experience with the UltraWide-bore 900-MHz NMR magnet. *IEEE Trans Appl Supercond* 2015;**25**(3):1-5.
22. Kok MB, Hak S, Mulder WJM, Van Der Schaft DWJ, Strijkers GJ, Nicolay K. Cellular compartmentalization of internalized paramagnetic liposomes strongly influences both T1 and T2 relaxivity. *Magn Reson Med* 2009;**61**(5):1022-1032.
23. Rosenberg JT, Kogot JM, Lovingood DD, Strouse GF, Grant SC. Intracellular bimodal nanoparticles based on quantum dots for high-field MRI at 21.1 T. *Magn Reson Med* 2010;**64**(3):871-882.
24. Lockman PR, Koziara JM, Mumper RJ, Allen DD. Nanoparticle surface charges alter blood-brain barrier integrity and permeability. *J Drug Target* 2004;**12**(9–10):635-641.
25. Sastre RL, Olmo R, Teijón C, Muñíz E, Teijón JM, Blanco MD. 5-fluorouracil plasma levels and biodegradation of subcutaneously injected drug-loaded microspheres prepared by spray-drying poly(d,l-lactide) and poly(d,l-lactide-co-glycolide) polymers. *Pharm* 2007;**338**(1–2):180-190.
26. Yen SY, Sung KC, Wang JJ, Yoa-Pu Hu O. Controlled release of nalbuphine propionate from biodegradable microspheres: in vitro and in vivo studies. *Pharm* 2001;**220**(1–2):91-99.
27. Yang F, Lim GP, Begum AN, Ubeda OJ, Simmons MR, Ambegaokar SS, et al. Curcumin inhibits formation of amyloid β oligomers and fibrils, binds plaques, and reduces amyloid in vivo. *J Biol Chem* 2005;**280**(7):5892-5901.
28. Goel A, Kunnumakkara AB, Aggarwal BB. Curcumin as "Curecumin": from kitchen to clinic. *Biochem Pharmacol* 2008;**75**(4):787-809.
29. Lim GP, Chu T, Yang F, Beech W, Frautschy S a, Cole GM. The curry spice curcumin reduces oxidative damage and amyloid pathology in an Alzheimer transgenic mouse. *J Neurosci* 2001;**21**(21):8370-8377.
30. Zhang L, Fiala M, Cashman J, Sayre J, Espinosa A, Mahanian M, et al. Curcuminoids enhance amyloid-beta uptake by macrophages of Alzheimer's disease patients. *J Alzheimers Dis* 2006;**10**(1):1-7.
31. Sah H, Thoma LA, Desu HR, Sah E, Wood GC. Concepts and practices used to develop functional PLGA-based nanoparticulate systems. *Nanomedicine* 2013;**8**:747-765.
32. Poduslo JF, Hultman KL, Curran GL, Preboske GM, Chamberlain R, Marjańska M, et al. Targeting vascular amyloid in arterioles of Alzheimer disease transgenic mice with amyloid β protein antibody-coated nanoparticles. *J Neuropathol Exp Neurol* 2011;**70**(8):653-661 [Internet, Available from: http://www.pubmedcentral.nih.gov/articlerender.fcgi?artid=4749027&tool=pmcentrez&rendertype=abstract%5Cnhttp://jnen.oxfordjournals.org/lookup/doi/10.1097/NEN.0b013e318225038c].
33. Cheng KK, Chan PS, Fan S, Kwan SM, Yeung KL, Wáng YXJ, et al. Curcumin-conjugated magnetic nanoparticles for detecting amyloid plaques in Alzheimer's disease mice using magnetic resonance imaging (MRI). *Biomaterials* 2015;**44**:155-172.
34. Ayton S, Fazlollahi A, Bourgeat P, Raniga P, Ng A, Lim YY, et al. Cerebral quantitative susceptibility mapping predicts amyloid-β-related cognitive decline. *Brain* 2017;**140**(8):2112-2119.

AUTHOR QUERY FORM

ELSEVIER	**Journal: NANO** **Article Number: 1876**	**Please e-mail your responses and any corrections to:** **E-mail: Corrections.ESCH@elsevier.spitech.com**

Dear Author,

Please check your proof carefully and mark all corrections at the appropriate place in the proof (e.g., by using on-screen annotation in the PDF file) or compile them in a separate list. Note: if you opt to annotate the file with software other than Adobe Reader then please also highlight the appropriate place in the PDF file. To ensure fast publication of your paper please return your corrections within 48 hours.

For correction or revision of any artwork, please consult http://www.elsevier.com/artworkinstructions.

We were unable to process your file(s) fully electronically and have proceeded by

☐ Scanning (parts of) your article ☐ Rekeying (parts of) your article ☐ Scanning the artwork

Any queries or remarks that have arisen during the processing of your manuscript are listed below and highlighted by flags in the proof. Click on the 'Q' link to go to the location in the proof.

Location in article	**Query / Remark: click on the Q link to go** **Please insert your reply or correction at the corresponding line in the proof**
Q1	Your article is registered as a regular item and is being processed for inclusion in a regular issue of the journal. If this is NOT correct and your article belongs to a Special Issue/Collection please contact m.farooqui@elsevier.com immediately prior to returning your corrections.
Q2	The author names have been tagged as given names and surnames (surnames are highlighted in teal color). Please confirm if they have been identified correctly.
Q3	Correctly acknowledging the primary funders and grant IDs of your research is important to ensure compliance with funder policies. We could not find any acknowledgement of funding sources in your text. Is this correct?
Q4, Q5	Please supply page range. Please check this box if you have no corrections to make to the PDF file. ☐

Thank you for your assistance.